Ferro-spin-glass domain model for disordered Ni-Mn

J. S. Kouvel, W. Abdul-Razzaq, and Kh. Ziq
Department of Physics, University of Illinois at Chicago, Chicago, Illinois 60680
(Received 11 August 1986)

A ferro-spin-glass (FSG) domain model, recently developed for a Ni-Mn reentrant spin-glass (SG) alloy, is applied here to several Ni-Mn compositions on either side of the multicritical point (MCP). From displaced hysteresis loops measured after cooling in fields strong enough to saturate the thermoremanence, the values deduced for both the average domain magnetization (M_S) and the unidirectional domain anisotropy field (H_K) decrease steadily with increasing Mn concentration, showing no anomaly at the composition of the MCP. However, as deduced from symmetrical loops measured after zero-field cooling (assuming the same M_S and H_K), the average exchange field for the net antiferromagnetic coupling between adjacent domains (H_E) remains small (<600 Oe) in the reentrant SG regime but rises very rapidly as the Mn concentration increases past the MCP composition. Nevertheless, in this critical composition region, H_E is consistently much weaker than the average exchange field within the domains, implying that the FSG domain boundaries coincide with surfaces over which the spin frustration is especially severe. Essentially the same characteristic variation of H_E with alloy composition is deduced separately from the observed changes in the displaced hysteresis loops for different fields applied during cooling. Recent electron-spin-resonance data for Ni-Mn cooled in zero and large fields are seen to be consistent with a FSG-domain-model interpretation of these different thermomagnetic conditions.

I. INTRODUCTION

The disordered Ni-Mn alloy of 23 at. % Mn, which becomes ferromagnetic at $T_C \approx 160$ K, undergoes a "reentrant" transition at $T_{fg} \approx 60$ K marked by the appearance of irreversible and time-dependent magnetization properties characteristic of a spin-glass state.[1] In particular, when the alloy is cooled to 4.2 K from above T_{fg} in a sufficiently large field ($H_{\rm cool}$), its magnetic hysteresis loop is completely displaced from the origin, such that the magnetization associated with the saturated (but slowly time decaying) thermoremanence reverses rapidly at nearly the same negative field ($-H_c$) for both branches of the loop. Thus, the $H_{\rm cool}$-induced anisotropy is almost purely unidirectional, and, consistent with recent theory,[2-5] this was seen to imply that the sample is acting as a single ferro-spin-glass (FSG) domain with a net ferromagnetic moment, whose reversal corresponds to a rigid (elastic) rotation of all the spins against the collective restoring action of Dzyaloshinsky-Moriya-type interactions. From this viewpoint, the symmetrical hysteresis loop obtained for zero $H_{\rm cool}$—where the magnetization varies rapidly near $\pm H_c$, reaches high-field values comparable to those of the displaced loop, but then returns essentially to the origin—was seen to suggest that in the zero-$H_{\rm cool}$ condition the sample is subdivided into smaller but similar FSG domains with randomly oriented anisotropy fields.[1] That the macroscopic magnetization process is via domain rotation had been concluded earlier from low-temperature magnetoresistance data on a similarly reentrant Ni-Mn alloy.[6]

Further study of $Ni_{77}Mn_{23}$ showed that the shape of the zero-$H_{\rm cool}$-hysteresis loop does not quite conform to a simple FSG-domain picture, and it was initially thought that the domain anisotropy fields may be preferentially oriented along the length of the rod-shaped sample.[7] However later measurements on a spherical sample of the same alloy yielded zero-$H_{\rm cool}$ loops of very similar shape; hence, an alternative explanation for the discrepancy was considered.[8] Specifically, an exchange coupling between the domains (heretofore neglected) was included in the analysis, and a very reasonable data fit was attained under the model conditions that the average interdomain coupling is weakly antiferromagnetic and that each domain interacts predominantly with neighboring domains of oppositely directed anisotropy fields. Under these conditions, a rapid but continuous spin-flop-like process occurs around a critical value of the applied field, thereby producing an S-shaped hysteresis loop that resembles the measured zero-$H_{\rm cool}$ loop for $Ni_{77}Mn_{23}$.

We have now investigated the applicability of the FSG domain model to disordered Ni-Mn alloys of higher (from 23 up to 27) at. % Mn. According to the magnetic phase diagram presented in the preceding paper,[9] this composition range extends through a multicritical point located at 23.9 at. % Mn, beyond which (at higher at. % Mn) the spin-glass state disorders (at T_g) directly into the paramagnetic state with no intervening ferromagnetism. In this normal spin-glass (SG) regime, the magnetic properties of Ni-Mn closely resemble those of Cu-Mn, the arcetypal SG alloy system. Especially relevant in this comparison are the displaced hysteresis loops of field-cooled Cu-Mn, whose rapid magnetization reversals have been interpreted as the coordinated motion of large interacting groups of spins,[10,11] which may be thought to constitute magnetic "domains."[11] In the present paper, the displaced

hysteresis loops and related low-temperature properties of Ni-Mn are shown to demonstrate that FSG domains continue to exist in the normal SG regime and, moreover, that the model parameters describing the domains vary systematically with alloy composition, even through that of the multicritical point.

II. RESULTS AND DISCUSSION

A. Hysteresis loops for saturated-thermoremanent-magnetization and zero-H_{cool} conditions

The disordered Ni-Mn alloy samples used in this study were the same as those described in the preceding paper[9]—namely, of 23, 23.5, 24, 24.5, 25, 26, and 27 at. % Mn— and their magnetizations (M) were similarly measured with a vibrating-sample magnetometer. Initially, hysteresis loops were obtained for each sample after cooling to 4.2 K from above T_{fg} or T_g (the temperature for the onset of magnetic irreversibility in the reentrant or normal SG regime[9]) in a field (H_{cool}) strong enough to saturate the thermoremanent magnetization (TRM). For the samples of 23 to 25 at. % Mn, $H_{cool}=10$ kOe was sufficient, while for 26 at. % Mn, TRM saturation required $H_{cool}=25$ kOe. In the case of 27 at. % Mn, the TRM was still rising at our highest attainable H_{cool} (~ 60 kOe); this sample was therefore ignored for the rest of this study.

The hysteresis loops obtained for the saturated-TRM condition are displayed in Fig. 1 as M versus the demagnetization-corrected field (H). In each case, the negative horizontal displacement of the loop from the origin greatly exceeds the small separation between its two branches. Together with the rapidity of the magnetization reversals at negative H (which probably would be

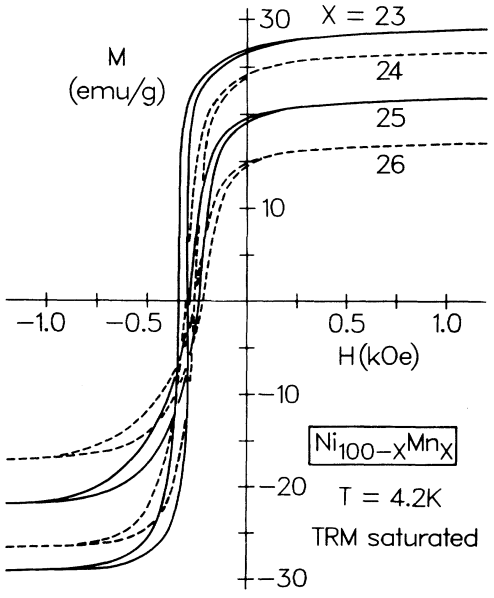

FIG. 1. Magnetic hysteresis loops for various Ni-Mn alloys in saturated-TRM condition after field-cooling to 4.2 K. Loops for 23.5 and 24.5 at. % Mn are omitted for clarity.

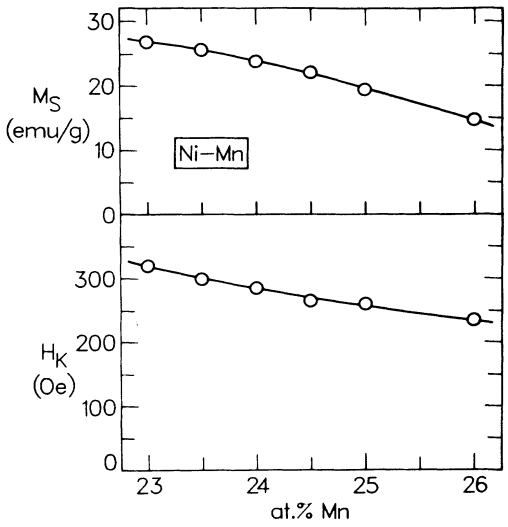

FIG. 2. Average domain magnetization (M_S) and unidirectional anisotropy field (H_K) vs Ni-Mn alloy composition.

even more rapid if the samples were spherical rather than rod-shaped[8]), this behavior suggests a rigid collective rotation of all the spins against unidirectional anisotropy forces. Hence, as previously observed for 23 at. % Mn,[8] each of the alloy samples in this condition appears to be acting as a single ferro-spin-glass (FSG) domain with a net ferromagnetic moment (M_S) essentially equal to the saturated TRM and a unidirectional anisotropy field ($\mathbf{H}_K$) whose magnitude is the negative of the average coercive field and whose direction is that of $\mathbf{H}_{cool}$. As seen in Fig. 1 for M_S and H_K thus defined, both these parameters decrease slowly (especially H_K) and steadily with increasing at. % Mn. The values of M_S and H_K are plotted versus alloy composition in Fig. 2 and are so listed in Table I. The remarkable nonfeature is that both these parameters vary smoothly through the composition of the multicritical point (23.9 at. % Mn),[9] showing no anomaly in passing from the reentrant to the normal SG regime.

It should be noted that M_S is consistently well below the value of ~ 95 emu/g, which would correspond to a ferromagnetic alignment of all the atomic moments in these alloys.[12] The smallness of M_S testifies to the frustrated spin arrangement within the FSG domains, which

TABLE I. Domain-model parameters (and susceptibilities) for $Ni_{100-x}Mn_x$.

x (at. %)	M_S (emu/g)	H_K (Oe)	H_E (Oe)	χ_0 (10^{-4} emu/g Oe)
23	26.9	320	250	219
23.5	25.7	300	405	155
24	24.1	285	540	118
24.5	22.2	265	1080	61
25	19.6	260	3460	18.2
26	14.8	235	6205	7.8

presumably derives from a coexistence of ferromagnetic Ni-Ni and Ni-Mn interactions and antiferromagnetic Mn-Mn interactions between neighboring atomic spins.[13–16] The increasing prevalence of the latter interactions with increasing at. % Mn can explain qualitatively the observed decrease of M_S. Moreover, that some of the spins are extremely frustrated (thus experiencing very weak net exchange fields) is indicated in Fig. 1 by the slow but continued rise of M with increasing positive H.

In our next set of experiments, the hysteresis loop of each Ni-Mn sample was measured after cooling to 4.2 K in zero field. Since the loops for this zero-H_{cool} condition are symmetric about the origin, they are shown in Fig. 3 for positive H only. In each case, the maximum field of measurement was kept below the threshold field for the onset of an isothermal remanent magnetization (IRM).[1] Hence, the loops in Fig. 3 show essentially no remanence; in fact, M is nearly reversible at all H. Considering the shape of the loop for 23 at. % Mn, we observe (as was noted earlier[7,8]) that an initial low-field linearity is followed successively by upward and downward curvatures. This characteristic variation clearly persists for the alloys of higher at. % Mn but with decreasing initial slope and with the inflection point moving to higher fields, which, for 25 and 26 at. % Mn, exceed the maximum fields allowable for zero IRM. Thus, although the zero-IRM criterion prevents us from following all these loops up to high M, they appear amenable to the same model interpretation as that previously proposed in the case of 23 at. % Mn.[8]

Specifically, the zero-H_{cool} loop for $Ni_{77}Mn_{23}$ was seen to suggest that the sample is subdivided into many FSG domains, each of them similar to the single domain for the saturated-TRM condition, but with the anisotropy fields (H_K) of the different domains orientated at random. Furthermore, the characteristic S shape of the zero-H_{cool} loop was found to be interpretable in terms of a weak antiferromagnetic exchange field (H_E) of coupling between adjacent domains. However, in applying this model to the rest of the zero-H_{cool} loops in Fig. 3, we are restricted experimentally to their behavior at low M, effectively to their initial slopes (or susceptibilities) for which the FSG domain model gives[8]

$$\chi_0=(2M_S/3)/(H_K+2H_E)\ . \tag{1}$$

The values of χ_0 taken from the initial slopes of these loops are listed in Table I. Substituting these values and those for M_S and H_K into Eq. (1), we solve for the average interdomain exchange field H_E, whose values are plotted versus alloy composition in Fig. 4 and are also listed in Table I. Clearly, H_E increases monotonically with increasing at. % Mn, but its increase is very slow up to 24 at. % Mn (approximately the multicritical-point composition), where it accelerates and proceeds to rise much more rapidly. Thus, unlike M_S and H_K, which vary gradually over this whole composition range (Fig. 2), H_E shows very different quantitative variations in the reentrant and normal SG regimes.

It should be noted that even though H_E reaches over 6 kOe at 26 at. % Mn, its values in this composition range are at least 2 orders of magnitude smaller than the average exchange field *within* the domains, as estimated from the fact that the magnetic ordering temperatures are consistently above 100 K.[9] Thus, it appears that the boundaries between the FSG domains are located at surfaces over which, on average, the net exchange coupling is relatively very weak.

B. Hysteresis loops for intermediate-H_{cool} conditions

Our discussion thus far regarding FSG-domain boundaries has pertained specifically to Ni-Mn samples in a zero-H_{cool} condition. It is reasonable to assume that a similar situation exists in these samples for a nonzero H_{cool} that is too weak to saturate the TRM (i.e., to pro-

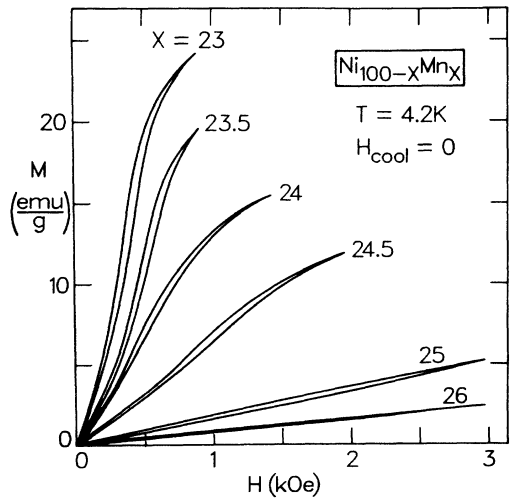

FIG. 3. Magnetic hysteresis loops for various Ni-Mn alloys after zero-field cooling to 4.2 K.

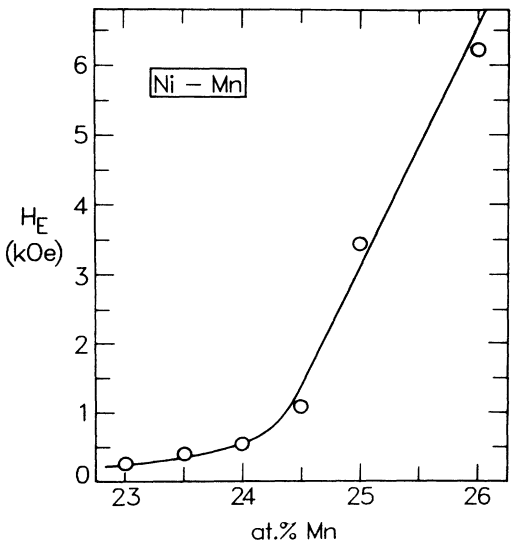

FIG. 4. Average exchange field for interdomain coupling (H_E) vs Ni-Mn alloy composition.

duce a single FSG domain) but gives rise to a multidomain configuration with a preferential (nonrandom) orientation of the domain anisotropy field ($\mathbf{H}_K$). If this assumption is valid, it will allow us an alternative experimental method for determining H_E and thus provide a check on our original estimates.

To develop this method, we must extend the FSG-domain model[8] so that it applies for intermediate H_{cool}. It will again be taken that the alloy sample consists of domain aggregates, within each of which adjacent domains have opposite-directed anisotropy fields ($\mathbf{H}_K$), and that the $\mathbf{H}_K$ axes of the different aggregates are oriented randomly. For $H_{\text{cool}}=0$, the configuration is assumed to be isotropic, where the domain aggregates of different $\mathbf{H}_K$ axes are of equal volume fraction and the domains of opposite $\mathbf{H}_K$ within each aggregate are also equal in volume fraction. This configuration is shown schematically in Fig. 5(a). Also shown in this figure is the corresponding configuration envisaged for nonzero H_{cool} after it has been removed to yield an unsaturated TRM. Here, the domains with $\mathbf{H}_K$ parallel to $\mathbf{H}_{\text{cool}}$ have grown in volume at the expense of those with $\mathbf{H}_K$ antiparallel or perpendicular to $\mathbf{H}_{\text{cool}}$. Defining the magnetizations of these three types of domains as M_1, M_2, and M_3, respectively, and ignoring (for simplicity) all other orientations of $\mathbf{H}_K$, we set as a reasonable but arbitrary approximation

$$M_1=(1+5\alpha)M_S/6\ ,$$
$$M_2=(1-\alpha)M_S/6\ , \tag{2}$$
$$M_3=(1-\alpha)M_S/3\ ,$$

where the volume-fraction parameter α can vary between 0 and 1. In general, for any α, Eq. (2) gives $M_1+M_2+2M_3=M_S$, the scalar magnetization per unit volume throughout the sample, and $M_1-M_2=\alpha M_S=M_R$, the remanent magnetization parallel to $\mathbf{H}_{\text{cool}}$. For $\alpha=1$, $M_1=M_S$ and $M_2=M_3=0$, corresponding to the single FSG domain of the saturated-TRM condition, whereas for $\alpha=0$, $M_1=M_2=M_S/6$ and $M_3=M_S/3$, corresponding to the "isotropic" zero-H_{cool} condition.[17]

In Fig. 5(b), the domain magnetizations ($\mathbf{M}_1,\mathbf{M}_2,\mathbf{M}_3$) for the nonzero-$H_{\text{cool}}$ condition are shown in their rotational response to an external field $\mathbf{H}$ applied opposite to $\mathbf{H}_{\text{cool}}$; their orientations relative to $\mathbf{H}_{\text{cool}}$ are specified by the angles ϕ_1, ϕ_2, and ϕ_3, respectively. For an aggregate of domains with $\mathbf{H}_K$ parallel or antiparallel to $\mathbf{H}_{\text{cool}}$, as represented by the "longitudinal-H_K" configuration in the upper half of the figure, the magnetic energy may be written as

$$E_L=-(H+H_K)M_1\cos\phi_1-(H-H_K)M_2\cos\phi_2 + \tfrac{1}{2}H_E(M_1+M_2)\cos(\phi_1+\phi_2)\ , \tag{3}$$

where positive H is along $\mathbf{H}_{\text{cool}}$, and H_E is the exchange field representing the antiferromagnetic coupling between the domains of oppositely directed $\mathbf{H}_K$. Minimization of E_L with respect to ϕ_1 and ϕ_2 gives

$$(H+H_K)M_1\sin\phi_1-\tfrac{1}{2}H_E(M_1+M_2)\sin(\phi_1+\phi_2)=0 \tag{4a}$$

and

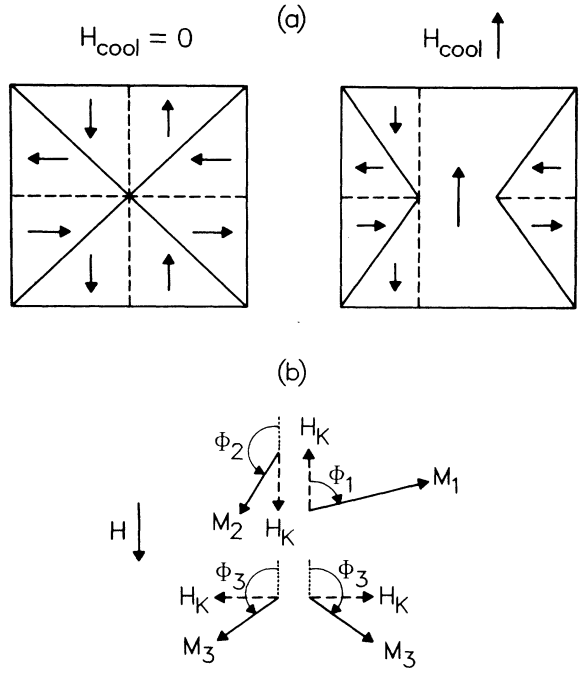

FIG. 5. (a) Schematic domain configurations for zero-field-cooled and field-cooled conditions; arrows represent domain anisotropy fields (and domain magnetizations in zero applied field). (b) Response of domain magnetizations (solid vectors) to applied field opposite to $\mathbf{H}_{\text{cool}}$; dashed vectors are domain anisotropy fields.

$$(H-H_K)M_2\sin\phi_2-\tfrac{1}{2}H_E(M_1+M_2)\sin(\phi_1+\phi_2)\ 0\ , \tag{4b}$$

respectively, whose simultaneous solutions for ϕ_1 and ϕ_2 at different H determine the magnetization of this configuration parallel to $\mathbf{H}$,

$$M_L=M_{L1}+M_{L2}=M_1\cos\phi_1+M_2\cos\phi_2\ . \tag{5}$$

Analogously, for an aggregate of domains with $\mathbf{H}_K$ in opposite directions normal to $\mathbf{H}_{\text{cool}}$, as represented by the "transverse-H_K" configuration in the lower half of Fig. 5(b), the magnetic energy is

$$E_T=-2HM_3\cos\phi_3-2H_KM_3\sin\phi_3+H_EM_3\cos2\phi_3\ , \tag{6}$$

whose minimization with respect to ϕ_3 gives

$$H\sin\phi_3-H_K\cos\phi_3-H_E\sin2\phi_3=0\ , \tag{7}$$

from which the solutions for ϕ_3 at different H determine the configuration magnetization parallel to $\mathbf{H}$,

$$M_T=2M_3\cos\phi_3\ . \tag{8}$$

In all these expressions, M_1, M_2, and M_3 are taken to follow Eq. (2) in their dependences on α (which rises from 0 to 1 with increasing H_{cool}).

As a numerical example, we consider the case of $H_E/H_K=2$ and $\alpha=0.25$. Equations (2)–(8) are used in calculating M_{L1}, M_{L2}, and M_T (each normalized by M_S)

as a function of H/H_K, and the results are plotted in Fig. 6(a). As expected, M_T varies linearly through the origin and gradually saturates at high positive and negative H, where $\cos\phi_3 \rightarrow \pm 1$ and $M_T \rightarrow \pm 2(1-\alpha)M_S/3 = \pm 0.5M_S$. The variations of M_{L1} and M_{L2} are more complicated and interesting. At $H=0$, where $\phi_1=0$ and $\phi_2=\pi$, it follows that $M_{L1}=(1+5\alpha)M_S/6=0.375M_S$ and $M_{L2}=-(1-\alpha)M_S/6=-0.125M_S$, and this situation persists at positive and negative H out to $H'(+)$ and $H'(-)$, respectively. At $H'(+)$, M_{L2} starts to reverse and become positive, while M_{L1} changes accommodatingly (due to the antiferromagnetic coupling) and returns to its original positive value. At $H'(-)$, it is M_{L1} that starts to reverse (and become negative) and M_{L2} that changes accommodatingly (and returns to its original negative value). The critical fields $H'(\pm)$ are found to correspond to the roots of the quadratic equation,

$$2M_1M_2(H')^2-(M_1^2-M_2^2)H_EH' -2M_1M_2H_K^2-(M_1+M_2)^2H_EH_K=0 , \quad (9)$$

which, from the dependences of M_1 and M_2 on α in Eq. (2), gives for small α ($\geqq 0$),

$$H'(\pm)=\pm(H_K^2+2H_EH_K)^{1/2}+3\alpha H_E , \quad (10)$$

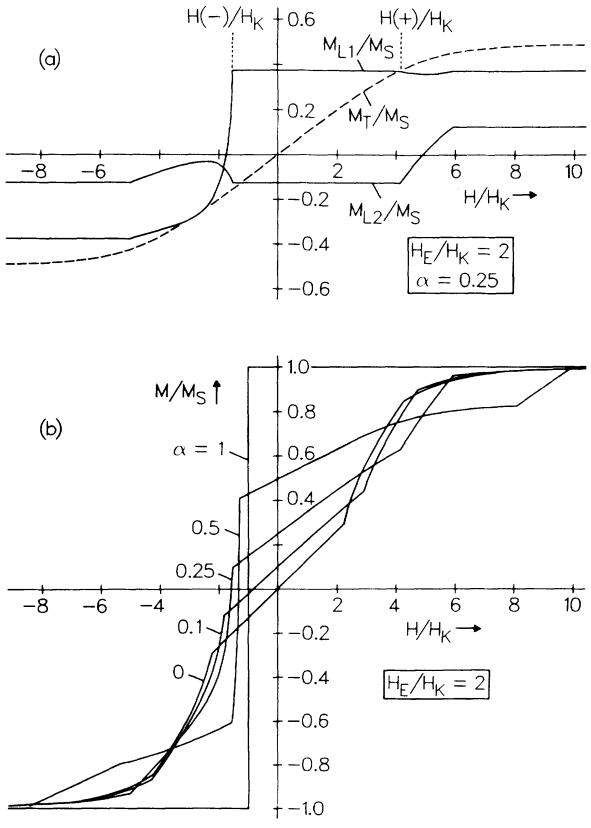

FIG. 6. (a) Normalized domain magnetizations versus H/H_K, calculated as discussed in text; locations of normalized critical fields $H'(\pm)/H_K$ are indicated. (b) Normalized total magnetization versus H/H_K for different volume-fraction parameters (α).

and for large α ($\leqq 1$),

$$H'(+)=\tfrac{1}{2}[6(1-\alpha)^{-1}-5]H_E+H_K , \quad H'(-)=-\tfrac{1}{3}(4-\alpha)H_K . \quad (11)$$

Equation (10), which was derived earlier[8] for $\alpha=0$, shows that as α increases from 0, $H'(+)$ becomes more positive and $H'(-)$ less negative. As α approaches 1, Eq. (11) shows that $H'(+)$ goes to plus infinity while $H'(-)$ rises to $-H_K$. Note that the latter equation is valid only for $H_E \neq 0$. For $H_E=0$, we see from Eq. (9) that $H'(\pm) = \pm H_K$ for any α. Hence, any variation of $H'(\pm)$ with α reflects the existence of H_E, and we shall be exploiting this important feature.

The above calculations were repeated for $\alpha=0$, 0.1, 0.5, and 1, with H_E/H_K kept equal to 2. For each α, the total magnetization M ($=M_{L1}+M_{L2}+M_T$) is plotted (normalized by M_S) against H/H_K in Fig. 6(b). In each case except for $\alpha=0$, there is a remanent magnetization $M_R(=\alpha M_S)$, from which M varies asymmetrically for positive and negative H, giving rise to a displaced hysteresis loop (of zero width, since the model includes no dissipation). Note especially that, as H decreases from zero, M decreases gradually until H reaches $H'(-)$, where M starts abruptly to decrease faster. As α rises from 0 to 1, the gradual change of M becomes slower while $H'(-)$ and M_R increase, and these effects combine to cause the negative coercive field to vary with M_R nonmonotonically. However, the variation of $H'(-)$ with M_R is monotonic and, therefore, is a more practical standard of comparison with experiment.

It must be mentioned that the sharpness of various features of the calculated curves in Fig. 6(b) is an artifact of the simplifyingly limited number of $\mathbf{H}_K$ orientations considered in the present analysis. The curve for $\alpha=0$ previously derived from a proper averaging over all $\mathbf{H}_K$ orientations[8] is considerably smoother than the $\alpha=0$ curve shown here. Nevertheless, many of the distinctive features of the curves in Fig. 6(b) are readily identifiable in the experimental results for Ni-Mn that we will now be presenting.

Displayed in Fig. 7 are the hysteresis loops of our Ni-Mn samples of 23, 24.5, and 25 at.% Mn, measured after cooling to 4.2 K in different H_{cool}; H has again been corrected for demagnetization. In each case, the remanent magnetization M_R (i.e., the TRM) is found to saturate at $H_{\text{cool}} \approx 10$ kOe, but it is evident that the approach to saturation as a function of H_{cool} becomes very much slower at higher at.% Mn, as observed earlier.[1] Except for zero H_{cool}, all the loops are displaced from the origin, and they are all fairly narrow in width. The average coercive field (H_c) is seen to have its highest negative value at low H_{cool} and to slowly decrease in magnitude with increasing H_{cool} (and M_R), ultimately reaching the limiting value shown earlier in Fig. 1. This variation of H_c is qualitatively very similar to that shown by the calculated curves in Fig. 6(b), and it clearly gets larger with increasing at.% Mn.

However, the feature of the experimental loops in Fig. 7 that is most amenable to our model interpretation is the "shoulder" at which M starts to drop rapidly with increasing negative H, whose location in H can be identified

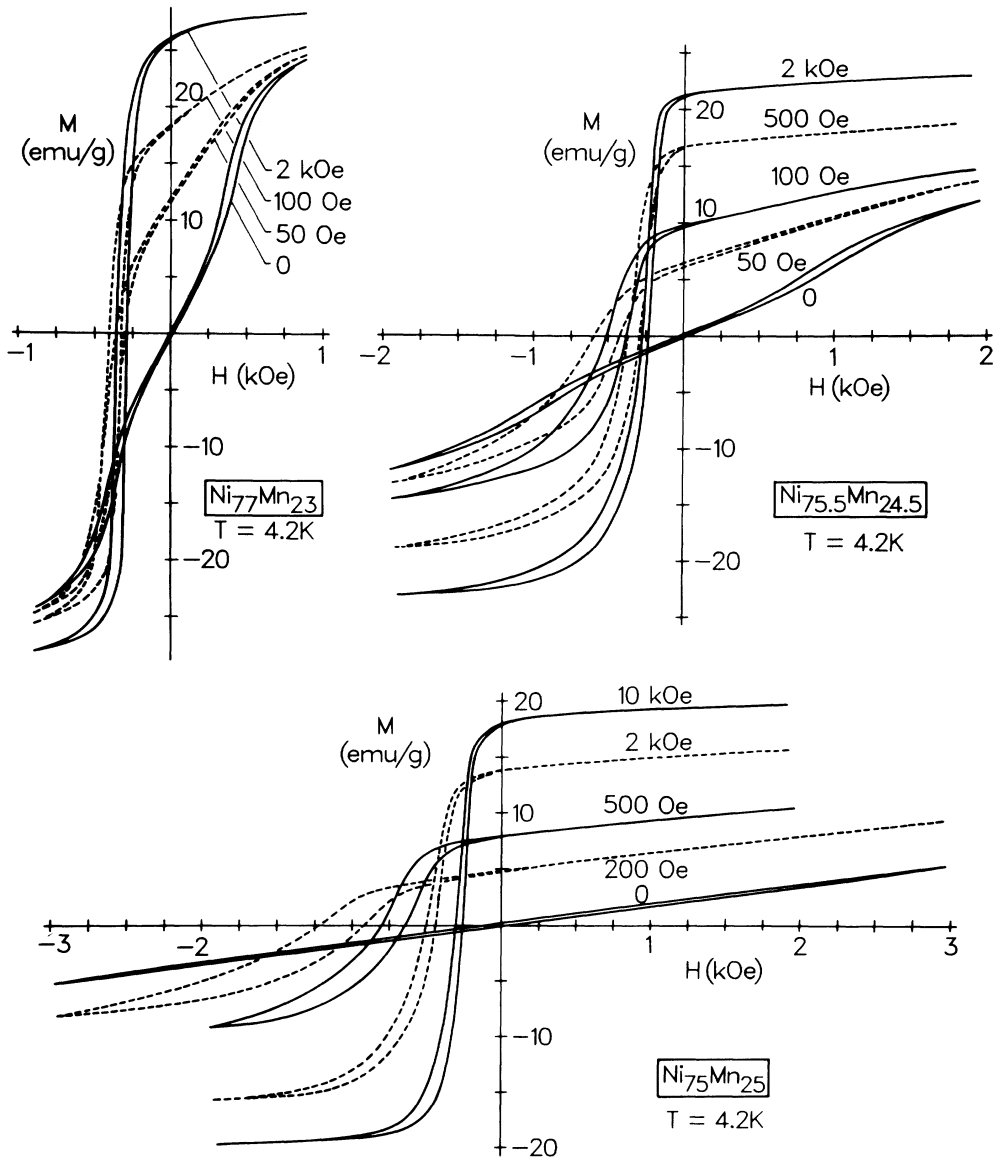

FIG. 7. Magnetic hysteresis loops for various Ni-Mn alloys after cooling to 4.2 K in different fields (including zero).

with $H'(-)$ in the model. Since the "shoulder" of each loop is fairly rounded, we adopted a simple consistent procedure for specifying its location. As demonstrated in Fig. 8 for one of the experimental loops, we extend a tangent line from the inflection point of each branch until it intersects a tangent line from the remanence (M_R) point. The points of intersection, labeled H'_1 and H'_2, are then averaged to give $H'(-)$, henceforth referred to simply as H'.

For each alloy, the negative experimental values of H' obtained by this procedure were normalized by H_K, which is the limiting magnitude of H' as M_R approaches its saturation value M_S. Plotted in Fig. 9 is M_R/M_S versus H'/H_K, and in each case, as M_R/M_S decreases from unity, H'/H_K becomes increasingly more negative. The total

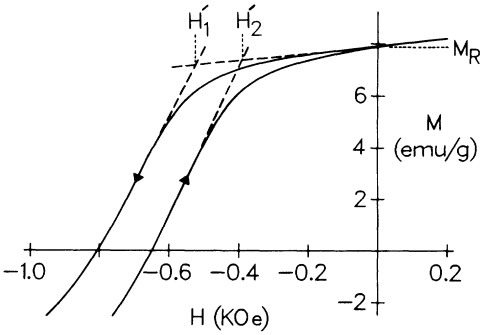

FIG. 8. Illustration of graphical procedure for determining critical field H' (average of H'_1 and H'_2) from measured hysteresis loop (for $Ni_{75}Mn_{25}$ cooled to 4.2 K in 500 Oe).

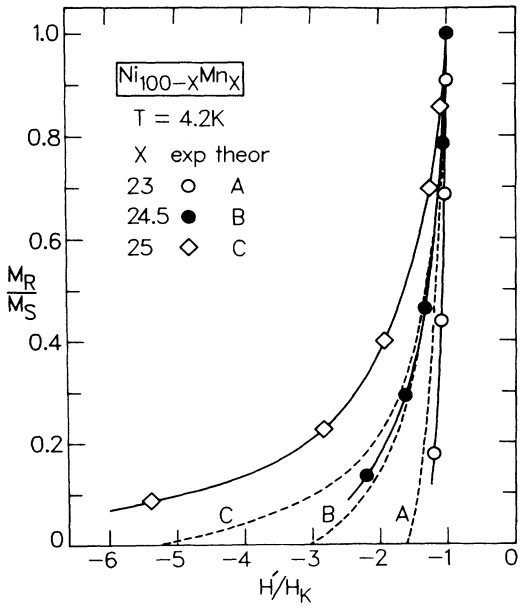

FIG. 9. Experimental (solid) and calculated (dashed) curves of M_R/M_S versus H'/H_K for various Ni-Mn alloys.

variation of H'/H_K is very small for 23 at. % Mn but gets progressively much larger for 24.5 and 25 at. % Mn. For a model comparison, we have calculated M_R/M_S versus H'/H_K from Eq. (9), using the values of H_E and H_K listed for these three alloys in Table I. The calculated curves are shown dashed in Fig. 9, where they clearly display monotonic variations very similar to those of the experimentally derived curves. Since within the model any variations of H' with M_R derive entirely from the existence of H_E, the agreement between the two sets of curves constitutes a confirmation of our original results regarding the dependence of H_E on alloy composition, as depicted in Fig. 4.

The only quantitative disagreement of note between the two sets of curves in Fig. 9 is in the case of 25 at. % Mn, where the experimental curve shows a larger variation of H'/H_K. This discrepancy could signify that the value of H_E for this alloy is actually larger than the value originally deduced from χ_0, the initial slope of the zero-$H_{\rm cool}$ loop (Fig. 3). In our original analysis, no subtraction was made from χ_0 of the intrinsic susceptibility of each domain, which can be estimated approximately from the residual slope of the high-$H_{\rm cool}$ loop (Fig. 1) at high positive H. For the alloys of <25 at. % Mn, the subtraction would be negligible, but for higher at. % Mn, where χ_0 is rather small, the subtraction could result in a significantly higher value of H_E. Hence, it may well be that the rise of H_E in the normal SG regime is even more rapid than appears in Fig. 4.

III. CONCLUDING REMARKS

Despite the approximate nature of the FSG domain model described here and earlier,[8] its three parameters (M_S,H_K,H_E) appear to capture the basic aspects of the reentrant and normal SG states of disordered Ni-Mn. While M_S and H_K are averages of the net ferromagnetic moments and the unidirectional anisotropy fields for the FSG domains comprising the sample, H_E is an exchange field that represents the average net coupling between neighboring domains. The values of both M_S and H_K are found to vary smoothly with composition through that of the multicritical point (Fig. 2), whereas the values deduced for H_E show little change in the reentrant SG regime but then rise rapidly when the composition enters the normal SG regime with increasing at. % Mn (Fig. 4). Moreover, throughout this critical composition region, H_E is much weaker (by over two orders of magnitude) than the average net exchange field within the domains, thus showing that the domain boundaries coincide with surfaces of very high spin frustration.

The location of the domain boundaries and the size distribution of the FSG domains with different orientations of $\mathbf{H}_K$ vary with the thermomagnetic history of the sample. Indeed, when cooled in a field ($H_{\rm cool}$) strong enough to saturate the TRM, the sample acts essentially as a single FSG domain with $\mathbf{H}_K$ parallel to $\mathbf{H}_{\rm cool}$. For lower $H_{\rm cool}$, domains of other $\mathbf{H}_K$ orientations appear, and ultimately for zero $H_{\rm cool}$, domains of all $\mathbf{H}_K$ orientations are equally represented, resulting in a zero remanent magnetization. However, for Ni-Mn alloys in the reentrant SG regime, the zero-remanence state pertains specifically to a sample of nonzero demagnetization, because in this regime the time-independent $M(H_{\rm cool})$ curves are found to manifest a spontaneous magnetization ($M_{\rm sp}$) in zero internal field.[9] Since $M_{\rm sp}$ is smaller than the saturated TRM, the time-independent $M_{\rm sp}$ state presumably corresponds to some multidomain configuration with a preferential orientation of $\mathbf{H}_K$. It would also follow that the characteristic time decay of the saturated TRM involves the creation and growth of FSG domains of different $\mathbf{H}_K$.

Apart from the magnetization evidence, the existence of FSG domains in disordered Ni-Mn can also be seen to be reflected in recent electron-spin-resonance (ESR) data. In particular, from low-temperature ESR spectra obtained for $Ni_{74}Mn_{26}$, it was found[18] that for $H_{\rm cool}=+10$ kOe the resonances are quite sharp and the positive and negative fields for resonance are asymmetrically disposed, such that $H_r(+)<-H_r(-)$, whereas for $H_{\rm cool}=0$ the asymmetry is absent and the resonances are much broader, extending roughly from $\pm H_r(+)$ to $\mp H_r(-)$ with reference to the field-cooled resonance fields. In the former case, the asymmetry of the resonance fields was attributed[18] to a "macroscopic anisotropy field" parallel to $\mathbf{H}_{\rm cool}$, which we can readily identify with the $\mathbf{H}_K$ of a single FSG domain. Correspondingly, we can ascribe the broad resonances in the latter case to a multidomain situation involving all directions of $\mathbf{H}_K$, as described above. Clearly, however, further ESR experiments on Ni-Mn are needed for a comprehensive test of the FSG domain model.

For the FSG domain model to be applicable, most of the frustrated spins in each domain must be coupled together so strongly (e.g., by Heisenberg-type interactions) that an applied field will cause them and their net magnetization to turn rigidly and elastically against the rela-

tively weak Dzyaloshinksy-Moriya-type forces that produce the unidirectional domain anisotropy.[2–5] Such a situation prevails at sufficiently low temperatures in Ni-Mn and also presumably in Cu-Mn and Ag-Mn, which exhibit similarly narrow and displaced hysteresis loops upon field cooling.[19,20] In other SG alloy systems such as Au-Fe, field cooling produces broad undisplaced loops,[21] which would imply that the Dzyaloshinsky-Moriya-type interactions are relatively strong, causing the spins individually (or in small groups) to flip inelastically in an applied field. In such cases, different thermomagnetic sample preparations may still result in different FSG domain configurations, but the domains do not remain intact during any subsequent changes in field, unless perhaps the changes are fairly small. Ni-Mn itself probably evolves into such a case with increasing temperature—for which the field-cooled hysteresis loop is seen to widen and concurrently lose its displacement[22]—and we plan to investigate this evolution and the associated changes in the FSG domain structure.

ACKNOWLEDGMENTS

We are grateful for many helpful discussions with I. A. Campbell, A. Fert, F. Hippert, H. Hurdequint, K. Levin, P. Monod, and W. M. Saslow at the outset of this study. Our work has been supported by the National Science Foundation under Grant No. DMR-84-06898.

[1]W. Abdul-Razzaq and J. S. Kouvel, J. Appl. Phys. **55**, 1623 (1984).
[2]P. M. Levy, C. Morgan-Pond, and A. Fert, J. Appl. Phys. **53**, 2168 (1982).
[3]C. L. Henley, H. Sompolinsky, and B. I. Halperin, Phys. Rev. B **25**, 5849 (1982).
[4]W. M. Saslow, Phys. Rev. B **27**, 6873 (1983).
[5]C. M. Soukoulis, G. S. Grest, and K. Levin, Phys. Rev. B **28**, 1510 (1983).
[6]S. Senoussi and Y. Oner, J. Magn. Magn. Mater. **40**, 12 (1983).
[7]W. Abdul-Razzaq and J. S. Kouvel, J. Appl. Phys. **57**, 3467 (1985).
[8]J. S. Kouvel and W. Abdul-Razzaq, J. Magn. Magn. Mater. **53**, 139 (1985).
[9]W. Abdul-Razzaq and J. S. Kouvel, preceding paper, Phys. Rev. B **35**, 1764 (1987).
[10]P. Monod, J. J. Prejean, and B. Tissier, J. Appl. Phys. **50**, 7324 (1979).
[11]C. N. Guy, J. Phys. F **12**, 1453 (1982).
[12]The atomic moments assumed are $0.3\mu_B$ for Ni and $3.2\mu_B$ for Mn, as determined for ordered Ni_3Mn by neutron diffraction; see C. G. Shull and M. K. Wilkinson, Phys. Rev. **97**, 304 (1955).
[13]W. J. Carr, Phys. Rev. **85**, 590 (1952).
[14]A. Z. Menshikov, V. A. Kazanisev, N. N. Kuzmin, and S. K. Sidorov, J. Magn. Magn. Mater. **1**, 91 (1975).
[15]M. Hennion, B. Hennion, and F. Kajzar, Solid State Commun. **21**, 231 (1977).
[16]T. J. Hicks and O. Moze, J. Phys. F **11**, 2633 (1981).
[17]Because of the limited number of $\mathbf{H}_K$ orientations considered for simplicity in the analysis, the symmetry of the zero-H_{cool} domain configuration is cubic rather than spherical.
[18]H. Hurdequint, J. S. Kouvel, and P. Monod, J. Magn. Magn. Mater. **31-34**, 1429 (1983).
[19]J. S. Kouvel, J. Phys. Chem. Solids **21**, 57 (1961).
[20]P. A. Beck, *Magnetism in Alloys,* edited by P. A. Beck and J. T. Waber (TMS-AIME, New York, 1972), p. 211.
[21]W. Abdul-Razzaq, J. S. Kouvel, and H. Claus, Phys. Rev. B **30**, 6480 (1984).
[22]J. S. Kouvel, *Material Research Society Symposia Proceedings* (Elsevier, New York, 1983), Vol. 19, p. 353.